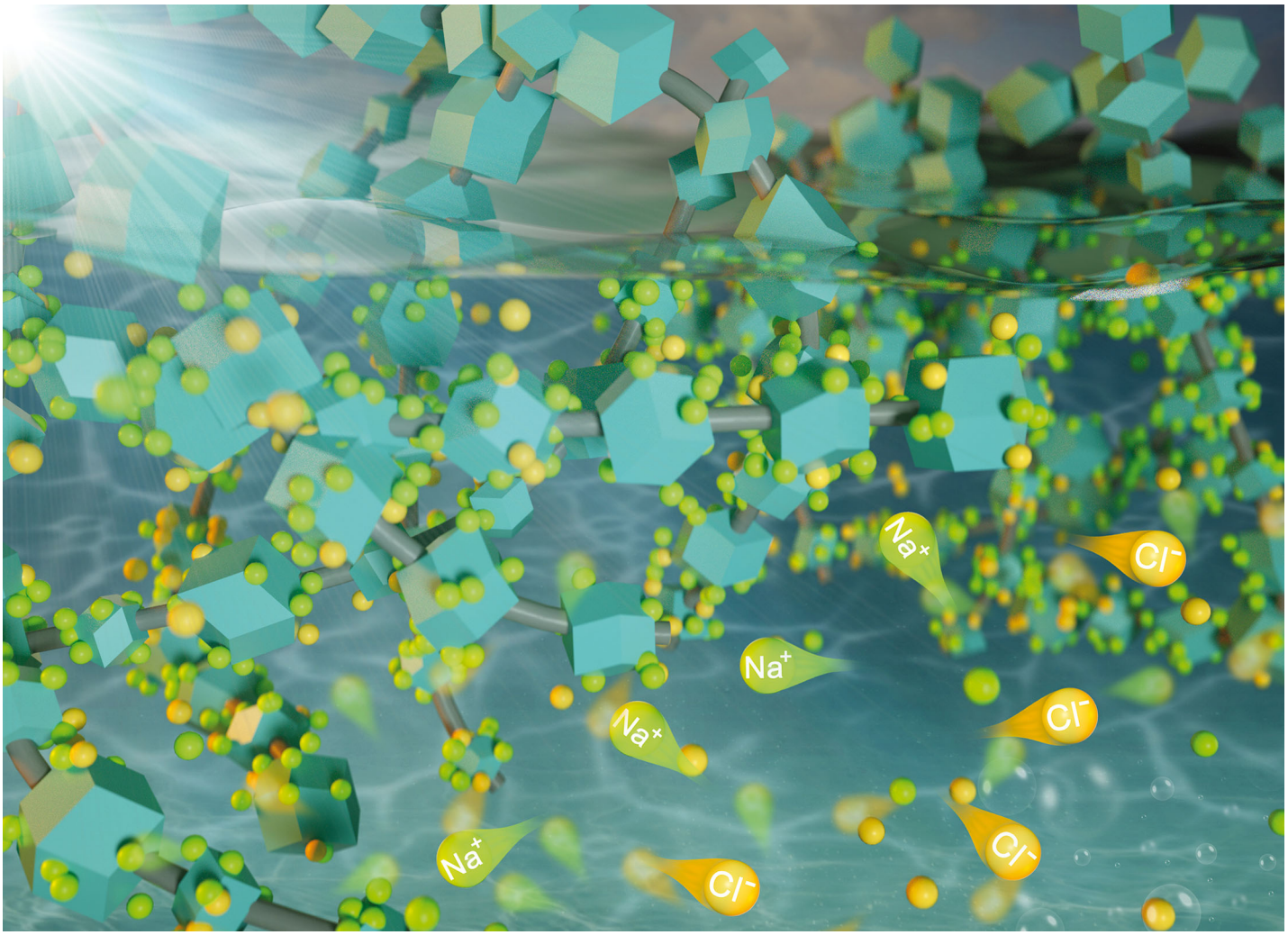

Showcasing the new capacitive deionization electrode family made up of metal–organic frameworks by Xingtao Xu at Hohai University, China, and Yusuke Yamauchi at The University of Queensland, Australia.

Nanoarchitectured metal–organic framework/polypyrrole hybrids for brackish water desalination using capacitive deionization

The metal–organic framework/polypyrrole hybrids highlight the first example of capacitive deionization electrodes derived from metal–organic framework-based materials.

As featured in:

See Xingtao Xu, Tao Yang, Yusuke Yamauchi *et al.*, *Mater. Horiz.*, 2019, **6**, 1433.

ROYAL SOCIETY OF CHEMISTRY | Celebrating IYPT 2019

rsc.li/materials-horizons

Registered charity number: 207890

Materials Horizons

COMMUNICATION

View Article Online
View Journal | View Issue

Cite this: *Mater. Horiz.*, 2019, 6, 1433

Received 25th February 2019,
Accepted 15th April 2019

DOI: 10.1039/c9mh00306a

rsc.li/materials-horizons

Nanoarchitectured metal–organic framework/polypyrrole hybrids for brackish water desalination using capacitive deionization†

Ziming Wang,‡[a] Xingtao Xu,‡*[a] Jeonghun Kim,[bc] Victor Malgras,[d] Ran Mo,[a] Chenglong Li,[a] Yuzhu Lin,[a] Haibo Tan,[d] Jing Tang,[c] Likun Pan,[e] Yoshio Bando,[cdfg] Tao Yang*[a] and Yusuke Yamauchi*[bch]

New families of materials that may potentially replace dominant carbon electrodes have emerged as a major research hotspot in the field of capacitive deionization (CDI). Here, we report a metal–organic framework (MOF)/polypyrrole (PPy) hybrid, in which conductive PPy nanotubes that are running through each MOF particle have the potential to increase the overall bulk electrical conductivity, thus promoting such a system as a good CDI electrode material. Consequently, the MOF/PPy hybrid shows a high desalination capacity of 11.34 mg g^{-1}, which is amongst those of state-of-the-art CDI electrodes. Moreover, the MOF/PPy hybrid also shows a superior desalination performance for brackish water and good cycling stability, far exceeding typical carbon-based benchmarks. This is the first example of CDI electrodes derived from direct MOF-based materials, highlighting the potential of these hybrid systems as promising materials beyond traditional carbon electrodes.

New concepts

Capacitive deionization (CDI) is an emerging technology combining energy storage and desalination based on electrical double layer theory. Previous efforts towards promoting the practical implementation of CDI have mainly focused on developing porous carbons that possess both good electrical conductivity and high specific surface area. Unfortunately, porous carbons have been shown to severely suffer from low desalination capacity and poor cycling stability. Developing new families of CDI electrodes that could overcome these drawbacks is highly desirable, and still remains in its infancy. In this article, we first show that metal–organic frameworks (MOFs) could be directly used as active materials in CDI without further carbonization. By introducing highly conductive polypyrrole nanotubes into the poorly conductive MOF particles, the electrical resistance of a bulk MOF electrode can be effectively reduced to further improve the desalination capacity and cycling stability of such a hybrid. It is believed that our work will not only herald the advent of a new generation of CDI electrodes, but will also shed light on new applications for MOFs.

Introduction

The scarce availability of freshwater is undoubtedly one of the most critical problems of the 21st century, along with demographic growth, climate change and environmental contamination.[1–8] The great demand of the population for affordable freshwater motivates the emergence of a number of water desalination techniques,[9–13] such as reverse osmosis, thermal distillation, electrodialysis, and capacitive deionization (CDI). Among them, CDI is a relatively new approach based on ion separation using electrical double layer (EDL) theory, with low energy consumption and no chemical additives, and is therefore environmentally friendly.[14–17]

Generally, the performance of CDI is tightly bonded to the electrical conductivity and specific surface area (SSA) of active materials.[18–21] However, materials with both high electrical conductivity and SSA are rare, as far as we know. The active materials thus far used in CDI are various porous carbons,[22–28] including activated carbon (AC), carbon nanotube (CNT), carbon nanofiber (CNF), mesoporous carbon (MPC), carbon

[a] State Key Laboratory of Hydrology-Water Resources and Hydraulic Engineering, Hohai University, 1 N. Xikang Rd, Nanjing 210-098, China. E-mail: xingtao.xu@hhu.edu.cn, tao.yang@hhu.edu.cn
[b] Key Laboratory of Eco-chemical Engineering, College of Chemistry and Molecular Engineering, Qingdao University of Science and Technology, Qingdao 266042, China
[c] School of Chemical Engineering and Australian Institute for Bioengineering and Nanotechnology (AIBN), The University of Queensland, Brisbane, QLD 4072, Australia. E-mail: y.yamauchi@uq.edu.au
[d] International Center for Materials Nanoarchitectonics (WPI-MANA) and International Center for Young Scientists (ICYS), National Institute for Materials Science (NIMS), 1-1 Namiki, Tsukuba, Ibaraki 305-0044, Japan
[e] Shanghai Key Laboratory of Magnetic Resonance, School of Physics & Materials Science, East China Normal University, 3663 N. Zhongshan Rd, Shanghai 200-062, China
[f] Institute of Molecular Plus, Tianjin University, No. 11 Building, No. 92 Weijin Road, Nankai District, Tianjin, 300072, P. R. China
[g] Australian Institute for Innovative Materials, University of Wollongong, Squires Way, North Wollongong, NSW 2500, Australia
[h] Department of Plant and Environmental New Resources, Kyung Hee University, 1732 Deogyeong-daero, Giheung-gu, Yongin-si, Gyeonggi-do 446-701, South Korea

† Electronic supplementary information (ESI) available. See DOI: 10.1039/c9mh00306a

‡ These authors contributed equally to this work.

nanosphere (CNS), reduced graphene oxide (RGO), biomass-derived carbon, and three-dimensional carbon architectures. But recent studies have shown that carbon electrodes can be easily oxidized during the CDI process,[29] which usually leads to poor cycling stability and limits their large-scale use. To address these issues, an effective solution is to explore new families of active materials that could make the best of both SSA and electrical conductivity. Metal–organic frameworks (MOFs) are one class of materials with high porosity far exceeding those of porous carbons.[30–32] Although the SSAs of MOFs have been reaching values up to $\sim$7000 m^2 g^{-1},[33] the use of MOFs in CDI applications has been restricted to the role of precursors for porous carbons *via* pyrolysis,[34–39] because of their poor electrical conductivity.

Here, we investigate for the first time a CDI electrode based on a MOF/polypyrrole (PPy) hybrid, in which conductive PPy nanotubes are running through MOF particles, thus reducing the overall bulk electrical resistance. The MOF/PPy hybrid was synthesized through a simple and mild procedure by utilizing conductive PPy nanotubes as nucleation centers for *in situ* MOF crystal growth. Consequently, the MOF particles are interconnected through the conductive PPy nanotubes, yielding a high desalination capacity of 11.34 mg g^{-1}. These results describe the first example of using MOFs directly in CDI electrodes without further carbonization, showcasing their potential in such applications.

Results and discussion

As a typical example, the famous zeolitic imidazolate framework-67 (ZIF-67) was selected for preparing the MOF/PPy hybrid in this work. The synthetic procedure is schematically illustrated in Fig. 1, and the detailed experimental process is described in the ESI.† Firstly, a certain amount of the pre-synthesized PPy nanotubes is uniformly dispersed into a $Co(NO_3)_2$ methanolic solution under ultrasonication. In this stage, the PPy nanotubes effectively adsorb the free Co^{2+} ions *via* electrostatic attraction,[40] and serve as nucleation sites for ZIF-67 crystals after further slow addition of a 2-methylimidazole (2-MeIM) methanolic solution. After 24 h reaction, the as-prepared ZIF-67/PPy hybrid can be directly used as a CDI active material.

The structure and morphology of the ZIF-67/PPy hybrid were characterized using a field-emission scanning electron microscope (FESEM) and transmission electron microscope (TEM). Fig. S1a (ESI†) exhibits the interconnected network structure of

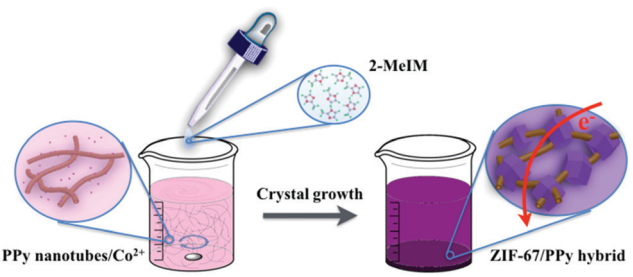

Fig. 1 Scheme illustrating the synthetic procedure of a ZIF-67/PPy hybrid.

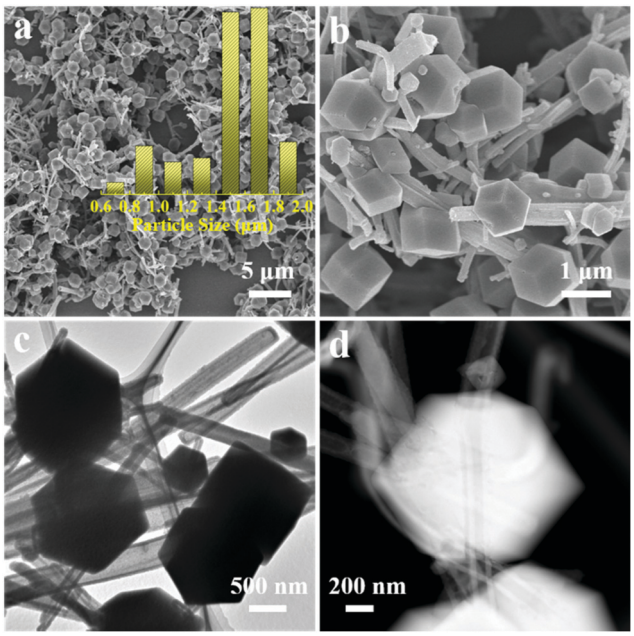

Fig. 2 (a and b) FESEM, (c) TEM, and (d) HAADF-STEM images of the ZIF-67/PPy hybrid. The inset of (a) shows the ZIF-67 particle size distribution.

the as-prepared PPy nanotubes. The diameter distribution is shown in the inset, with an average diameter of 230 $\pm$ 78 nm. The Fourier-transform infrared spectrum (Fig. S1b, ESI†) further confirms the high purity of the as-prepared PPy nanotubes. Subsequently, these nanotubes were used as substrates for growing ZIF-67 particles by the sequential addition of Co^{2+} ions and 2-MeIM (Fig. 2). Unlike the ZIF-67 particles, the ZIF-67/PPy hybrid benefits from the PPy nanotubes' three-dimensional network, interconnecting each MOF particle (Fig. 2a and b). The particle size distribution is shown in the inset of Fig. 2a, with an average size of 1.49 $\pm$ 0.28 μm. The TEM (Fig. 2c) and high-angle annular dark-field scanning TEM (HAADF-STEM, Fig. 2d) images further reveal that the ZIF-67/PPy hybrid is composed of well dispersed ZIF-67 polyhedra intertwined with the PPy nanotubes. In this structure, the PPy nanotubes run throughout the ZIF-67 crystals, serving as bridges for electrons to transfer between the MOF particles.[41,42]

The crystal structures of the PPy nanotubes, pure ZIF-67, and ZIF-67/PPy hybrid were first characterized by powder X-ray diffraction (XRD, Fig. 3a). The PPy nanotubes exhibit an amorphous nature with a broad hump corresponding to their repeating unit (*i.e.* pyrrole ring), indicating a highly oriented polymer chain.[43] The typical sharp diffraction peaks of both ZIF-67/PPy and pure ZIF-67 match the simulations, showcasing the high crystallinity of the MOF. In addition, no obvious diffraction peaks of the PPy nanotubes have been observed in the XRD pattern of ZIF-67/PPy. Only at excessively high PPy contents (increased up to 8-fold), an amorphous peak will be observed (Fig. S2, ESI†). N_2 adsorption/desorption isotherms were acquired to characterize the SSAs of the PPy nanotubes, pure ZIF-67, and ZIF-67/PPy hybrid (Fig. 3b). The SSA of the ZIF-67 particles decreases from 1719.6 to 1176.8 m^2 g^{-1} after forming the hybrid with the PPy nanotubes, which can

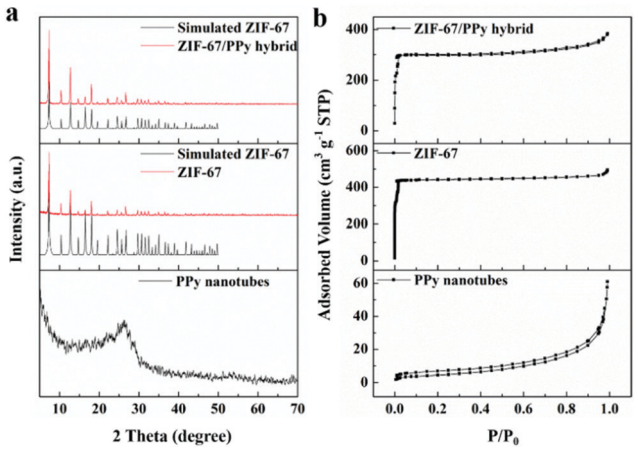

Fig. 3 (a) XRD patterns and (b) nitrogen sorption isotherms of the PPy nanotubes, ZIF-67 and ZIF-67/PPy hybrid.

be expected since the SSA of the pure PPy nanotubes is only 16.9 $m^2\ g^{-1}$.

Combining the high porosity and uniform micropores of ZIF-67 with the good electrical conductivity of PPy nanotubes makes such a hybrid a promising candidate for electrode materials. Electrochemical measurements were performed in a three-electrode configuration which utilizes an aqueous 1 M NaCl electrolyte, at a scan rate of 10 mV s^{-1} and in a potential window range of −0.2 V to 0.8 V (*vs.* Ag/AgCl). All cyclic voltammetry (CV) curves are rectangular-shaped with no evidence of redox peaks, indicating a typical capacitive behaviour (Fig. 4a). Additionally, the current density of the ZIF-67/PPy hybrid is much higher than those of the PPy nanotubes and ZIF-67, likely due to its superior capacitive properties.

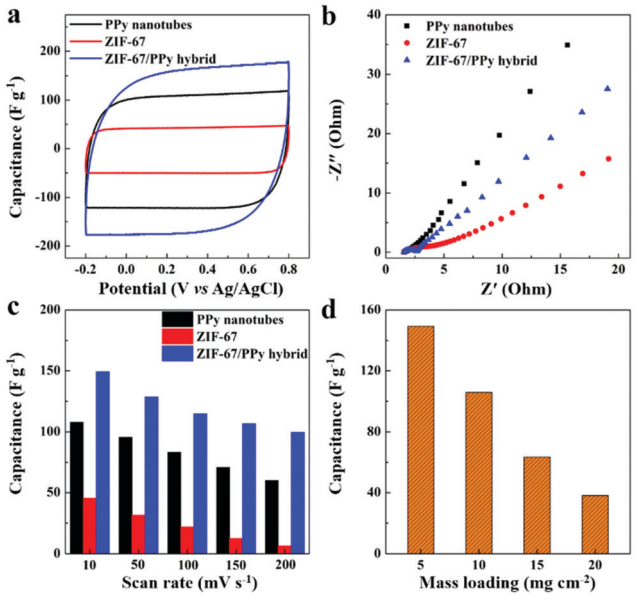

Fig. 4 Electrochemical performances of the PPy nanotubes, ZIF-67 and ZIF-67/PPy hybrid. (a) CV curves. (b) Nyquist impedance spectra. (c) Specific capacitances *vs.* scan rates. (d) Specific capacitance *vs.* mass loading of the ZIF-67/PPy hybrid.

Electrochemical impedance spectroscopy provides a useful way to study the intrinsic mechanisms responsible for improving the capacitive properties of the ZIF-67/PPy hybrid electrode. The Nyquist plots of all samples comprise a linear feature in the low frequency range and a small semicircle in the high frequency region (Fig. 4b). The charge transfer resistance (R_{ct}, obtained from the diameter of the semicircle) values of the samples are presented in Table S1 (ESI†). While the PPy nanotubes show a R_{ct} of 0.62 Ω, the resistance of ZIF-67 decreases from 3.20 to 1.32 Ω after hybridization, which is beneficial for faster charge transfer and greater charge storage within the electrode.

The specific capacitances *vs.* scan rates of all samples are shown in Fig. 4c. The ZIF-67/PPy hybrid shows a superior capacitance compared to the PPy nanotubes and pure ZIF-67 at the same scan rate, which can be ascribed to their low R_{ct} and relatively high SSA for ion adsorption. We also note that increasing the mass loading in the ZIF-67/PPy hybrid (Fig. 4d) results in a decrease of the specific capacitance, possibly due to the lower utilization efficiency of the active materials and the poorer electrical conductivity with the increase of mass loading.[41]

In general, high porosity and good electrical conductivity are two key factors in achieving high desalination capacity.[44] To study the desalination performance of our hybrid material, a CDI cell was assembled with two pairs of ZIF-67/PPy electrodes, and the performance was measured in 50 mL of aqueous NaCl solution with a starting concentration of 584 mg L^{-1} (corresponding to ∼10 mM) at 1.2 V. For comparison, CDI cells based on the PPy nanotubes and pure ZIF-67 were also built and characterized under identical conditions. As shown in Fig. 5a, once the operation voltage was fixed, the concentration of the NaCl solution decreased sharply before reaching a constant plateau. From eqn (S2) (see the ESI†), the desalination capacity of the ZIF-67/PPy hybrid is calculated to be 11.34 mg g^{-1}, which far exceeds those of the PPy nanotubes (6.92 mg g^{-1}) and pure ZIF-67 (3.82 mg g^{-1}). Such desalination capacity competes with those of state-of-the-art CDI electrodes (Table S2, ESI†), highlighting the potential of this hybrid. Fig. 5b shows that the ZIF-67/PPy hybrid exhibits a CDI Ragone plot that shifts towards higher desalination rates and capacities than for the PPy nanotubes and pure ZIF-67.

Experimental adsorption kinetics are compared to pseudo-first- and pseudo-second-order kinetic models in Fig. S3 (ESI†), respectively, and the results are presented in Table S3 (ESI†). Only the pseudo-first-order kinetic model fits the experimental data of the ZIF-67/PPy hybrid well, and the corresponding rate constant is 0.189, higher than that of ZIF-67 (0.163), likely due to the fast access of ions onto the surface through the interconnected structure.[45] Furthermore, the desalination capacity of the hybrid clearly increases as the NaCl concentration is varied from 1 to 10 mM (Fig. 5c). The ability of the hybrid to capture other metal ions (*e.g.* Na^+, K^+, Mg^{2+}, and Ca^{2+}) is also investigated. Under the same conditions (10 mM, 1.2 V), the electrosorption ability of the ZIF-67/PPy hybrid follows the order $Ca^{2+} > Mg^{2+} > K^+ > Na^+$ (Fig. 5d), possibly due to the combined effects of ionic charge and hydrated radius.[46]

To evaluate the practicability of our hybrid for brackish water desalination, a CDI cell with ten pairs of ZIF-67/PPy

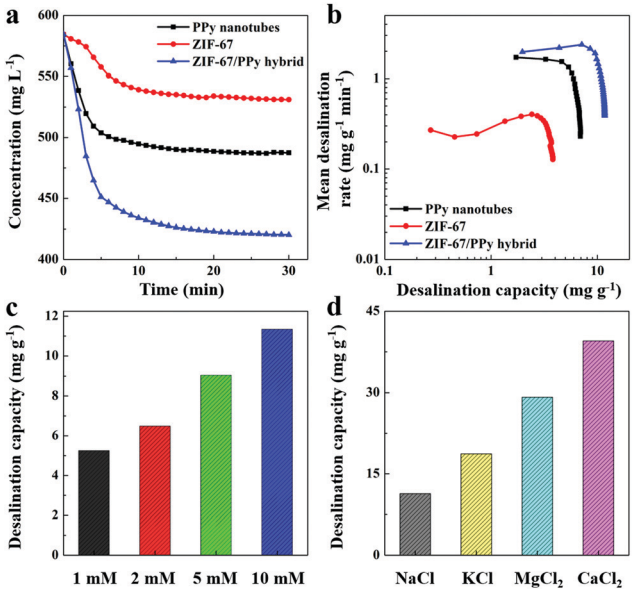

Fig. 5 (a) Salt concentration variations and (b) CDI Ragone plots of the PPy nanotubes, ZIF-67 and ZIF-67/PPy hybrid. CDI performances of the ZIF-67/PPy hybrid (c) at various NaCl concentrations and (d) in various metal ion solutions (10 mM).

electrodes was further studied in saline solution ($\sim$1530 mg L^{-1}). Typical carbons, such as AC (SSA: 2000–2500 m^2 g^{-1}), CNT (outer diameter: 10–20 nm, inner diameter: 5–10 nm, length: 10–30 μm, SSA: >200 m^2 g^{-1}), CNF (diameter: 400–500 nm, SSA: $\sim$850 m^2 g^{-1}), MPC (pore diameter: 3.8–4 nm, SSA: $\geq$900 m^2 g^{-1}), CNS (diameter: 300–400 nm, SSA: $\sim$450 m^2 g^{-1}), and RGO (SSA: $\sim$450 m^2 g^{-1}), were also investigated for comparison. The hydrophilicity of all samples was studied, as shown in Fig. S4 (ESI†). Interestingly, the hydrophilicity of the ZIF-67/PPy hybrid electrode is comparable to those of the other typical carbons, which is highly desirable for CDI application. Moreover, the ZIF-67/PPy hybrid shows a higher desalination performance (Fig. 6a and b) and superior cycling stability without obvious degradation after 100 cycles (Fig. 6c).

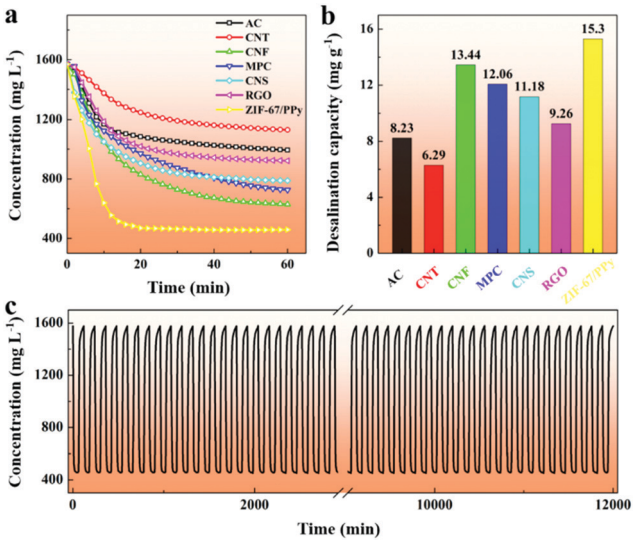

Fig. 6 (a) Salt concentration variations and (b) the corresponding desalination capacities of the ZIF-67/PPy hybrid along with typical carbon materials: AC, CNT, CNF, MPC, CNS, and RGO. (c) Cyclic concentration variation of a ZIF-67/PPy hybrid-based CDI cell.

Conclusions

In summary, a ZIF-67/PPy hybrid was prepared and employed as a CDI electrode material for the first time. It combines the high porosity and regular micropores of ZIF-67 with the high electrical conductivity of the PPy nanotubes, which thus endow the ZIF-67/PPy hybrid with a high desalination capacity of 11.34 mg g^{-1}, competing with the best-performance CDI electrodes. As a result of a practicability test, the ZIF-67/PPy hybrid-based CDI cell exhibits a superior desalination performance for high-concentration saline water, along with good cycling stability, far exceeding the typical carbon-based benchmarks.

Conflicts of interest

There are no conflicts to declare.

Acknowledgements

The work was jointly supported by the Fundamental Research Funds for the Central Universities (B18020057), and the grants from the National Natural Science Foundation of China (51879068, 41561134016), and the National Key Research and Development Program (2018YFC0407900). This work was also supported by the Australian Research Council (ARC) Future Fellow (FT150100479 and DE190101410). This work was performed in part at the Queensland node of the Australian National Fabrication Facility, a company established under the National Collaborative Research Infrastructure Strategy to provide nano- and micro-fabrication facilities for Australia's researchers.

Notes and references

1 T. Cui, T. Yang, C.-Y. Xu, Q. Shao, X. Wang and Z. Li, *Stoch. Environ. Res. Risk Assess.*, 2018, **32**, 1849–1866.
2 C.-S. Huang, T. Yang and H.-D. Yeh, *J. Hydrol.*, 2018, **561**, 277–285.
3 Z. Li, T. Yang, C.-S. Huang, C.-Y. Xu, Q. Shao, P. Shi, X. Wang and T. Cui, *Ecol. Indic.*, 2018, **89**, 356–364.
4 A. Kumar, T. Yang and M. P. Sharma, *Sci. Total Environ.*, 2019, **646**, 300–308.
5 X. Wang, T. Yang, B. Yong, V. Krysanova, P. Shi, Z. Li and X. Zhou, *Environ. Earth Sci.*, 2018, **77**, 465.
6 Y. Qin, D. Kavetski and G. Kuczera, *Water Resour. Res.*, 2018, **54**, 9637–9654.
7 Y. Qin, D. Kavetski and G. Kuczera, *Water Resour. Res.*, 2018, **54**, 9655–9683.
8 X. Wang, T. Yang, M. Wortmann, P. Shi, F. Hattermann, A. Lobanova and V. Aich, *Clim. Change*, 2017, **141**, 483–498.

9 G. Amy, N. Ghaffour, Z. Li, L. Francis, R. V. Linares, T. Missimer and S. Lattemann, *Desalination*, 2017, **401**, 16–21.
10 A. Subramani and J. G. Jacangelo, *Water Res.*, 2015, **75**, 164–187.
11 A. M. Lopez, M. Williams, M. Paiva, D. Demydov, T. D. Do, J. L. Fairey, Y. J. Lin and J. A. Hestekin, *Desalination*, 2017, **409**, 108–114.
12 J. Jin, X. Zhao, Y.-H. Du, M. Ding, C. Xiang, N. Yan, C. Jia, Z. Han and L. Sun, *iScience*, 2018, **6**, 289–298.
13 X. Sun, J. J. Park, H. S. Kim, S. H. Lee, S. J. Seong, A. S. Om and J. Y. Yoon, *Ultrason. Sonochem.*, 2018, **49**, 13–23.
14 X. Xu, Y. Liu, M. Wang, C. Zhu, T. Lu, R. Zhao and L. Pan, *Electrochim. Acta*, 2016, **193**, 88–95.
15 Z.-H. Huang, Z. Yang, F. Kang and M. Inagaki, *J. Mater. Chem. A*, 2017, **5**, 470–496.
16 F. Chen, Y. Huang, L. Guo, L. Sun, Y. Wang and H. Y. Yang, *Energy Environ. Sci.*, 2017, **10**, 2081–2089.
17 X. Xu, Z. Sun, D. H. C. Chua and L. Pan, *Sci. Rep.*, 2015, **5**, 11225.
18 X. Xu, L. Pan, Y. Liu, T. Lu and Z. Sun, *J. Colloid Interface Sci.*, 2015, **445**, 143–150.
19 T. Alencherry, A. R. Naveen, S. Ghosh, J. Daniel and R. Venkataraghavan, *Desalination*, 2017, **415**, 14–19.
20 F. Zhou, T. Gao, M. Luo and H. Li, *Chem. Eng. J.*, 2018, **343**, 8–15.
21 Z. Yue, T. Gao and H. Li, *Desalination*, 2019, **449**, 69–77.
22 Y. Li, J. Shen, J. Li, X. Sun, J. Shen, W. Han and L. Wang, *Carbon*, 2017, **116**, 21–32.
23 X. Xu, A. E. Allah, C. Wang, H. Tan, A. A. Farghali, M. H. Khedr, V. Malgras, T. Yang and Y. Yamauchi, *Chem. Eng. J.*, 2019, **362**, 887–896.
24 X. Xu, H. Tan, Z. Wang, C. Wang, L. Pan, Y. V. Kaneti, T. Yang and Y. Yamauchi, *Environ. Sci.: Nano*, 2019, **6**, 981–989.
25 K. Shi and I. Zhitomirsky, *Electrochim. Acta*, 2015, **174**, 588–595.
26 K. Shi, M. Ren and I. Zhitomirsky, *ACS Sustainable Chem. Eng.*, 2014, **2**, 1289–1298.
27 K. Shi, X. Yang, E. D. Cranston and I. Zhitomirsky, *Adv. Funct. Mater.*, 2016, **26**, 6437–6445.
28 X. Yang, K. Shi, I. Zhitomirsky and E. D. Cranston, *Adv. Mater.*, 2015, **27**, 6104–6109.
29 I. Cohen, E. Avraham, Y. Bouhadana, A. Soffer and D. Aurbach, *Electrochim. Acta*, 2013, **106**, 91–100.
30 J. Yu, C. Mu, B. Yan, X. Qin, C. Shen, H. Xue and H. Pang, *Mater. Horiz.*, 2017, **4**, 557–569.
31 C. Duan, J. Huo, F. Li, M. Yang and H. Xi, *J. Mater. Sci.*, 2018, **53**, 16276–16287.
32 C. Duan, F. Li, J. Xiao, Z. Liu, C. Li and H. Xi, *Sci. China Mater.*, 2017, **60**, 1205–1214.
33 O. K. Farha, I. Eryazici, N. C. Jeong, B. G. Hauser, C. E. Wilmer, A. A. Sarjeant, R. Q. Snurr, S. T. Nguyen, A. Ö. Yazaydın and J. T. Hupp, *J. Am. Chem. Soc.*, 2012, **134**, 15016–15021.
34 Y. Liu, X. Xu, M. Wang, T. Lu, Z. Sun and L. Pan, *Chem. Commun.*, 2015, **51**, 12020–12023.
35 M. Wang, X. Xu, J. Tang, S. Hou, M. S. A. Hossain, L. Pan and Y. Yamauchi, *Chem. Commun.*, 2017, **53**, 10784–10787.
36 X. Xu, M. Wang, Y. Liu, T. Lu and L. Pan, *J. Mater. Chem. A*, 2016, **4**, 5467–5473.
37 M. Wang, X. Xu, Y. Liu, Y. Li, T. Lu and L. Pan, *Carbon*, 2016, **108**, 433–439.
38 T. Gao, F. Zhou, W. Ma and H. Li, *Electrochim. Acta*, 2018, **263**, 85–93.
39 T. Gao, H. Li, F. Zhou, M. Gao, S. Liang and M. Luo, *Desalination*, 2019, **451**, 133–138.
40 V. Chandra and K. S. Kim, *Chem. Commun.*, 2011, **47**, 3942–3944.
41 X. Xu, J. Tang, H. Qian, S. Hou, Y. Bando, M. S. A. Hossain, L. Pan and Y. Yamauchi, *ACS Appl. Mater. Interfaces*, 2017, **9**, 38737–38744.
42 Y. Liu, N. Xu, W. Chen, X. Wang, C. Sun and Z. Su, *Dalton Trans.*, 2018, **47**, 13472–13478.
43 D. P. Dubal, N. R. Chodankar, Z. Caban-Huertas, F. Wolfart, M. Vidotti, R. Holze, C. D. Lokhande and P. Gomez-Romero, *J. Power Sources*, 2016, **308**, 158–165.
44 G. Wang, Q. Dong, T. Wu, F. Zhan, M. Zhou and J. Qiu, *Carbon*, 2016, **103**, 311–317.
45 X. Xu, L. Pan, Y. Liu, T. Lu, Z. Sun and D. H. C. Chua, *Sci. Rep.*, 2015, **5**, 8458.
46 M. Mossad and L. Zou, *J. Hazard. Mater.*, 2012, **213-214**, 491–497.